Single-atom Lasing in a Carbon-nanotube Quantum-dot

Yile Ying

June 6, 2019

Supervisor: Michele Governale

Abstract

We study the single-atom phonon-lasing effect in a system consisting of a mechanical oscillator (carbon-nanotube) and a quantum-dot in contact with two ferromagnetic leads. We show that, within rotation wave approximation and assuming uni-directional transport, the system exhibits sub-Poissonian statistics and reaches a non-equilibrium steady state with a non-zero phonon occupation number at resonance when the leads are sufficiently polarised and in antiparallel configuration. A diagrammatic perturbation expansion approach is developed to analyse the case where the leads are non-collinearly polarised. In the first order expansion, the results of the non-collinear case with different angles between polarisation of the two leads resemble those of the collinear case with different polarisation strength; the system behaves as a single-atom laser when the angle between the two magnetisations is sufficiently small and the leads are fully polarised.

Contents

1 Introduction

In contrast to conventional lasers, instead of exciting a large number of atoms to reach population inversion and obtain a coherent source of light, a single-atom laser only excites one atom and obtains nonclassical light [1]. The single-atom laser exhibits novel features like sub-Poissonian statistics [2], thresholdless lasing (i.e. lasing occurs with minimum pump powers) [3], and self-quenching (sometimes called antibunching) [4].

Since 1980s, scientists have coupled atoms like rubidium [5] and barium [6] with microwave photon cavities to create one-atom masers, or caesium with a high-finesse optical cavity [1] for a single-atom laser.

With the recent development of semiconductor and nanotechnology, single-atom lasing can also be demonstrated in systems with artificial atoms like quantum dots. It is shown both theoretically [7, 8, 9, 10] and experimentally [11, 12, 13, 14] that quantum dots coupled to microwave photon cavities can create micromasers.

The single-atom lasing effect can also be observed in systems with phonons instead of photons [15]. That is, instead of microwave photon cavities, we can couple quantum dots with mechanical resonators [16] such as the vibration modes of a carbon-nanotube [17, 18] to create phonon lasing.

In this project, we focus on the system proposed by Stadler, Belzig and Rastelli [19, 20]. The system consists of a carbon-nanotube quantum dot connected to two ferromagnetic leads. The dot spin states can couple to the vibration mode of the carbon-nanotube through the nanotube spin-orbit interaction and/or an external magnetic field gradient applied to the dot as shown in Figure (1). It has been demonstrated theoretically that lasing effect in this system can be achieved with collinearly polarised leads ($\hat{\mathbf{n}}_{\mathrm{L}} \parallel \hat{\mathbf{n}}_{\mathrm{R}}$) [21]. The aim of this project is to first reproduce this result, and then to explore the lasing phenomenon with non-collinearly polarised leads.

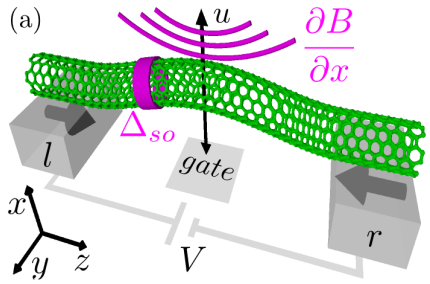

Figure 1: The set-up of the system with a carbon-nanotube quantum dot suspended between two magnetised leads. The spin-orbit interaction (Δ_{so}) of the nanotube and/or an external magnetic gradient ($\frac{\partial B}{\partial x}$) can couple the dot spin states with the vibration mode of the nanotube. Image source: [19, 20]

The report is organised as follows. In Section 2, we introduce the system and our basic assumptions (e.g. rotation wave approximation, uni-directional transport), derive the Hamiltonian and the Master Equation in the collinearly polarised case, and present the numerical simulation results with different collinear polarisation strength. In Section 3, we provide the adjustment to the Hamiltonian and the Master Equation when the leads are non-collinearly polarised, develop the diagrammatic rule to calculate transition rates in this case, and present the numerical simulation results. In the end we summarise the findings and discuss possible directions for future work.

2 Collinearly Polarised Leads

2.1 The Hamiltonian

There are four physical components in the set-up: a quantum-dot, a oscillator (the mechanical vibration of the carbon-nanotube), ferromagnetic leads connecting the nanotube, and a thermal bath as shown in Figure (2). Hence the Hamiltonian of the system describes these four components and the interactions between them:

$$\hat{H} = \hat{H}_{\mathrm{dot}} + \hat{H}_{\mathrm{osc}} + \hat{H}_{\mathrm{leads}} + \hat{H}_{\mathrm{bath}} + \hat{H}_{\mathrm{tun,leads}} + \hat{H}_{\mathrm{int,bath}} + \hat{H}_{\mathrm{int,dot}}.$$

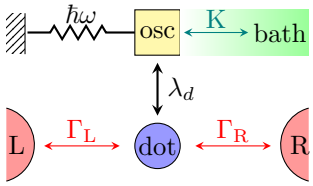

Figure 2: Schematic diagram of the system. The oscillation of the nanotube is modelled as a standard harmonic oscillator with a single vibration mode $\hbar\omega$. The oscillator is connected to a thermal bath with coupling strength $K \propto |\lambda_b|^2$. The quantum dot can exchange energy with the oscillator by flipping its spin, and this interaction strength is proportional to λ_d. The electron in the dot can tunnel to or from the leads with the tunnelling strength Γ, and $\Gamma_{\eta,\sigma} \propto |V_{\eta,\sigma}|^2$.

The vibration of the nanotube is modelled as a standard harmonic oscillator, and assumed to have a single vibration mode with energy $\hbar\omega$. Hence the Hamiltonian for the resonator is:

$$\hat{H}_{\text{osc}} = \hbar\omega \hat{b}^\dagger \hat{b},$$

where $\hat{b}^\dagger$ ($\hat{b}$) is the creation (annihilation) operator of the oscillator.

The oscillator interacts with the thermal bath, which has the Hamiltonian:

$$\hat{H}_{\text{bath}} = \sum_q \hbar\omega_q \hat{a}_q^\dagger \hat{a}_q,$$

where $\hat{a}_q^\dagger$ ($\hat{a}_q$) is the creation (annihilation) operator of phonons with energy $\hbar\omega_q$ in the bath. The bath is assumed to be in equilibrium at a temperature T_b. To study the lasing effect, we assume $T_b = 0$, hence the bath tends to bring the oscillator to its ground state. The interaction between the oscillator and the bath is:

$$\hat{H}_{\text{int,bath}} = \lambda_b \sum_q \left(\hat{a}_q^\dagger \hat{b} + \hat{b}^\dagger \hat{a}_q \right),$$

where λ_b is the interaction matrix element. In this work, the second term in $\hat{H}_{\text{int,bath}}$ always vanishes when applied to any states of the system as all the phonons in the bath are in the ground states.

When the leads are collinearly polarised, we can chose the quantisation axis of the dot spin to be parallel to the polarisation direction: $\hat{\mathbf{e}}_z \parallel \hat{\mathbf{n}}_{\text{L}} \parallel \hat{\mathbf{n}}_{\text{R}}$, and describe the quantum dot spin state as follows:

Dot State $\lvert\alpha\rangle$	$\lvert 0\rangle$	$\lvert\downarrow\rangle$	$\lvert\uparrow\rangle$	$\lvert\uparrow\downarrow\rangle$
Dot Energy E_α	0	$\epsilon_0 - \frac{\epsilon_z}{2}$	$\epsilon_0 + \frac{\epsilon_z}{2}$	$2\epsilon + U$

where U is the Coulomb interaction strength. Therefore, the Hamiltonian of the dot can be written as:

$$\hat{H}_{\text{dot}} = \sum_\sigma \epsilon_\sigma \hat{d}_\sigma^\dagger \hat{d}_\sigma + U \hat{d}_\uparrow^\dagger \hat{d}_\uparrow \hat{d}_\downarrow^\dagger \hat{d}_\downarrow,$$

where $\hat{d}_\sigma^\dagger$ ($\hat{d}_\sigma$) is the creation (annihilation) operator of the spin σ electron, $\epsilon_\uparrow = \epsilon_0 + \frac{\epsilon_z}{2}$ and $\epsilon_\downarrow = \epsilon_0 - \frac{\epsilon_z}{2}$.

The Hamiltonian for the leads is:

$$\hat{H}_{\text{leads}} = \sum_{\eta,\sigma,k} \epsilon_{k,\sigma} \hat{c}^{\dagger}_{\eta,\sigma,k} \hat{c}_{\eta,\sigma,k},$$

where $\hat{c}^{\dagger}_{\eta,\sigma,k}$ ($\hat{c}_{\eta,\sigma,k}$) is the creation (annihilation) operator of the spin σ electron with momentum of k in the η (= L, R) lead.

The electron can tunnel between the dot and the leads. The tunnelling matrix element is $V^{(*)}_{\eta,\sigma}$:

$$\hat{H}_{\text{tun,leads}} = \sum_{\eta,\sigma,k} \left(V_{\eta,\sigma} \hat{c}^{\dagger}_{\eta,\sigma,k} \hat{d}_{\sigma} + V^{*}_{\eta,\sigma} \hat{d}^{\dagger}_{\sigma} \hat{c}_{\eta,\sigma,k} \right)$$

The electron in the dot can exchange energy with the oscillator by flipping its spin, and this interaction can be characterised by:

$$\hat{H}_{\text{int,dot}} = -\lambda_d \left(\hat{d}^{\dagger}_{\downarrow} \hat{d}_{\uparrow} + \hat{d}^{\dagger}_{\uparrow} \hat{d}_{\downarrow} \right) \left(\hat{b}^{\dagger} + \hat{b} \right)$$

where λ_d is the interaction matrix element between the dot and the oscillator.

2.2 Eigenstates Under Rotation Wave Approximation

Our system of interest here is the coupled system of the dot and the oscillator. Hence we define the $\hat{H}_{sys} = \hat{H}_{dot} + \hat{H}_{osc} + \hat{H}_{int,dot}$.

We choose $|\alpha, n\rangle = |\alpha\rangle \otimes |n\rangle$ as the basis, where the spin state of the dot $\alpha = 0, \uparrow, \downarrow, \text{D}$, and the occupation of the oscillator $n = 0, 1, 2, \cdots$. $|D\rangle$ is defined as $\hat{d}^{\dagger}_{\uparrow} \hat{d}^{\dagger}_{\downarrow} |0\rangle$.

In this basis, the Hamiltonian of the interaction between the dot and the oscillator can be represented by:

$$\begin{aligned} \hat{H}_{\text{int,dot}} = -\lambda_d \sum_{n=0}^{\infty} (& \sqrt{n+1} \, |\downarrow, n+1\rangle \langle\uparrow, n| + \sqrt{n} \, |\uparrow, n\rangle \langle\downarrow, n+1| \\ & + \sqrt{n+1} \, |\uparrow, n+1\rangle \langle\downarrow, n| + \sqrt{n} \, |\downarrow, n\rangle \langle\uparrow, n+1|) \end{aligned} \tag{1}$$

When $|\lambda_d| \ll \hbar\omega \approx \epsilon_z$, the last two terms in Equation (1) can be neglected as the energy gap between $|\downarrow, n\rangle$ and $|\uparrow, n+1\rangle$ is much larger than the one between $|\uparrow, n\rangle$ and $|\downarrow, n+1\rangle$. Therefore, under the rotating wave approximation (RWA), the interaction Hamiltonian between the dot and the oscillator can be simplified to:

$$\hat{H}^{\text{RWA}}_{\text{int,dot}} = \lambda_d \sum_{n=0}^{\infty} \left(\sqrt{n+1} \, |\downarrow, n+1\rangle \langle\uparrow, n| + \sqrt{n} \, |\uparrow, n\rangle \langle\downarrow, n+1| \right)$$

Two of the eigenstates of $\hat{H}_{sys}$ are $|0, n\rangle$ and $|\text{D}, n\rangle$, with corresponding eigenenergies $\hbar\omega$ and $2\epsilon_0 + U + \hbar\omega n$, respectively.

The other two eigenstates are of superposition of $|\uparrow, n\rangle$ and $|\downarrow, n+1\rangle$:

$$|+, n\rangle = \sin\theta_n \, |\uparrow, n\rangle - \cos\theta_n \, |\downarrow, n+1\rangle$$

$$|-, n\rangle = \cos\theta_n \, |\uparrow, n\rangle + \sin\theta_n \, |\downarrow, n+1\rangle$$

where

$$\sin\theta_n = \frac{1}{\sqrt{2}}\sqrt{1-\frac{\Delta}{2\omega_n}},$$

$$\cos\theta_n = \frac{1}{\sqrt{2}}\sqrt{1+\frac{\Delta}{2\omega_n}},$$

and

$$\Delta = \hbar\omega - \epsilon_z,$$

$$w_n = \sqrt{\left(\frac{\Delta}{2}\right)^2 + \lambda_d^2\,(n+1)}.$$

The corresponding eigenvalues are

$$E_{\pm,n} = \epsilon_0 + \hbar\omega(n+\frac{1}{2}) \pm \omega_n.$$

We let $|\chi, n\rangle$ denote these eigenstates of the coupled Hamiltonian under RWA, where $\chi = 0, \mathrm{D}, +, -$, and $n = 1, 2, 3, \cdots$. When $n = 0$, besides the above four eigenstates, there is an extra eigenstate $|\downarrow, 0\rangle$. If there is an upper limit $n_{\max}$ for the occupation number, only three eigenstates exist for $n = n_{\max}$: $|0, n_{\max}\rangle$, $|D, n_{\max}\rangle$ and $|\uparrow, n_{\max}\rangle$. In this project, we set $n_{\max} = 100$, which is much larger than the average occupation number $\langle n\rangle$, thus it is large enough to capture the dynamics of the system and also not too big to save computational power during numerical simulation.

Note that the n here is no longer the oscillator occupation number when $\chi = \pm$; in fact, $\hat{b}^\dagger\hat{b}\,|\pm, n\rangle = \sin\theta_n n + \cos\theta_n(n+1)\,|\pm, n\rangle$.

2.3 Reduced Density Matrix and the Master Equation

We trace out the leads and the bath to obtain the reduced density matrix of our system of interest:

$$\hat{\rho} = \mathrm{Tr}_{\mathrm{leads,bath}}[\hat{\rho}_{full}] = \sum_{\chi,n} P_{\chi,n}\,|\chi, n\rangle\,\langle\chi, n|\,,$$

where $P_{\chi,n}$ is the probability of state $|\chi, n\rangle$ and $\sum_{\chi,n} P_{\chi,n} = 1$.

The Master Equation describing the time evolution of the probability is:

$$\dot{P}_{\chi,n} = \sum_{\chi',n'\neq\chi,n} \left(W_{\chi,n;\chi',n'}P_{\chi',n'} - W_{\chi',n';\chi,n}P_{\chi,n}\right),$$

where $W_{\chi,n;\chi',n'}$ is the transition rate from state $|\chi', n'\rangle$ to state $|\chi, n\rangle$. That is, the total change in the probability of being in state $|\chi, n\rangle$ equals the total transitions from other states to $|\chi, n\rangle$ minus the total transitions from $|\chi, n\rangle$ to other states.

For computational convenience, we define

$$W_{\chi,n;\chi,n} = -\sum_{\chi',n'\neq\chi,n} W_{\chi',n';\chi,n},$$

and the Master Equation can be simplified to

$$\dot{P}_{\chi,n} = \sum_{\chi',n'} W_{\chi,n;\chi',n'} P_{\chi',n'}. \tag{2}$$

In matrix form:

$$\dot{\boldsymbol{P}} = \boldsymbol{W}\boldsymbol{P}.$$

After sufficiently long time or when $t \to \infty$, we assume the system reaches a stationary state, which means, $\dot{P}_{\chi,n} = 0$ or $\dot{\boldsymbol{P}} = 0$. Therefore, the stationary state probability vector $\boldsymbol{P}_{sta}$ is the kernel of the transition rate matrix $\boldsymbol{W}$.

2.4 Transition Rates and Current

The transition rates between different states can be calculated via Fermi Golden Rule:

$$\begin{aligned} W_{\chi,n;\chi',n'} = &\sum_{\eta,\sigma} \Gamma_{\eta,\sigma} \left[f_\eta^+ \left(E_{\chi,n} - E_{\chi',n'} \right) | \left\langle \chi, n \right| d^\dagger \left| \chi', n' \right\rangle |^2 + f_\eta^- \left(E_{\chi',n'} - E_{\chi,n} \right) | \left\langle \chi, n \right| d \left| \chi', n' \right\rangle |^2 \right] \\ &+ \mathrm{K} | \left\langle \chi, n \right| b \left| \chi', n' \right\rangle |^2, \end{aligned} \tag{3}$$

where $f_\eta^+(E)$ is the Fermi function of the lead η, and $f_\eta^-(E) = 1 - f_\eta^+(E)$.

The first term in Equation (3) is due to electron tunnelling between the leads and the dot, and

$$\Gamma_{\eta,\sigma} = \frac{2\pi}{\hbar} |V_{\eta\sigma}|^2 \rho_{\eta\sigma}$$

where $\rho_{\eta\sigma}$ is the density of states for spin σ electrons in the lead η. Defining the polarisation of the lead η as $p_\eta = \frac{\rho_{\eta\uparrow} - \rho_{\eta\downarrow}}{\rho_{\eta\uparrow} + \rho_{\eta\downarrow}} \in [-1, 1]$, we can write $\Gamma_{\eta,\uparrow/\downarrow} = \Gamma_\eta (1 \pm p_\eta)$, where $\Gamma_\eta = \frac{\Gamma_{\eta\uparrow} + \Gamma_{\eta\downarrow}}{2}$. Let $\Gamma = \frac{\Gamma_L + \Gamma_R}{2}$, then $\Gamma_{L/R} = \Gamma(1 \pm a)$, where a describes the difference between the left and the right lead: $a = \frac{\Gamma_L - \Gamma_R}{\Gamma_L + \Gamma_R} \in [-1, 1]$. In the following analysis, we keep $a = 0$, i.e. $\Gamma_L = \Gamma_R = \Gamma$.

The second term in Equation (3) is due to the phonon tunnelling between the oscillator and the bath, and

$$\mathrm{K} = \frac{2\pi}{\hbar} |\lambda_b|^2 \rho_{\mathrm{bath}},$$

where ρ_{bath} is the phonon density of states in the bath.

A full list of transition rates between different states can be found in Appendix A.1, and the interactions between different components of the system can be seen in Figure (2)

We assume that electrons can only travel from the left lead to the right lead, i.e. $f_L^+(E) = 1$ and $f_R^+(E) = 0$. Under this assumption, the transition rates between the leads and the dot can be simplified to:

$$\begin{aligned} W_{\chi,n;\chi',n'} = &\sum_{\sigma} \left[\Gamma_{\mathrm{L},\sigma} | \left\langle \chi, n \right| d^\dagger \left| \chi', n' \right\rangle |^2 + \Gamma_{\mathrm{R},\sigma} | \left\langle \chi, n \right| d \left| \chi', n' \right\rangle |^2 \right] \\ &+ \mathrm{K} | \left\langle \chi, n \right| b \left| \chi', n' \right\rangle |^2. \end{aligned}$$

A full list of the transition rates under the uni-directional transport assumption can be found in Appendix A.2.

To calculate the current through the dot, we assign a factor of $e^{\mp i x_\eta}$ to each $f_\eta^{\pm}(E)$ term in the transition rates $W_{\chi,n;\chi',n'}$, where $|\chi, n\rangle \neq |\chi', n'\rangle$. The current can be calculated as:

$$I = ie\frac{\partial \boldsymbol{W}}{\partial x_L}\boldsymbol{P}|_{x_L=0} = -ie\frac{\partial \boldsymbol{W}}{\partial x_R}\boldsymbol{P}|_{x_R=0},$$

where e is the charge of an electron ($\approx 1.60217662 \times 10^{-19}$C).

2.5 Results

First we explore the case where the leads are fully polarised in antiparallel configuration, with the left lead having spin-up magnetisation and the right one having the opposite, i.e. $p = p_L = -p_R = 1$ and $\hat{n}_L = \hat{n}_R = \hat{e}_z$.

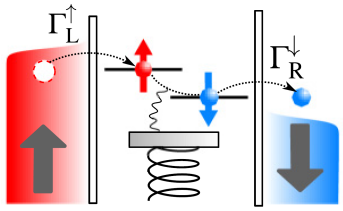

Figure 3: The electron travels from the left to the right lead by flipping its spin in the dot and giving away energy to the oscillator. The left lead is fully polarised to spin-up state and the right lead to spin-down state. Image source: [22].

With the uni-directional assumption mentioned before, in this antiparallel configuration with total polarisation, an electron can only tunnel from the left lead to the dot with its spin up. Hence it cannot tunnel to the right lead directly as the right lead only has spin down states available. However, as Figure (3) indicates, the electron in the quantum dot can flip its spin by interacting with the oscillator, and then tunnel to the right lead. This interaction can only happen when $E_{\downarrow,n+1} \approx E_{\uparrow,n}$, that is $\hbar\omega \approx \epsilon_z$, i.e. when the system is near or at resonance.

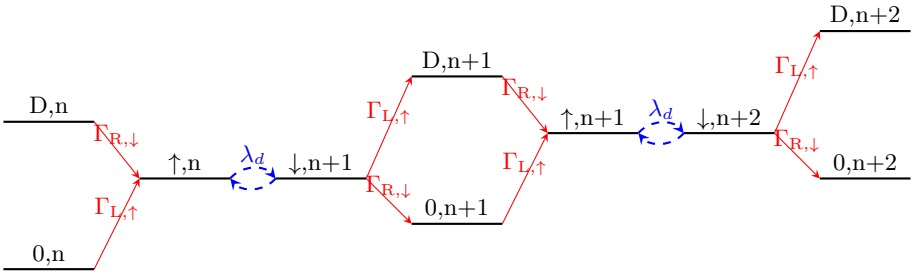

Figure 4: The dynamics contributing to the increase in the occupation number of the system. Thick lines are energy levels of state $|\alpha, n\rangle$. Red arrows are electron tunnellings when the leads are fully polarised in antiparallel configuration and under uni-directional transport assumption. Blue dashed arrows are the transitions due to the interaction between the dot and the oscillator. Here we assume $\epsilon_z = \hbar\omega$.

We can also analyse the dynamics using Figure 4. With the leads fully polarised in antiparallel configuration, the coupling to the leads and the interaction between the dot and the oscillator increase the phonon occupation number near or at resonance. Therefore, we expect the oscillator to heat up in this fully antiparallel magnetisation case, as long as the cooling effect of the thermal bath is sufficiently weak.

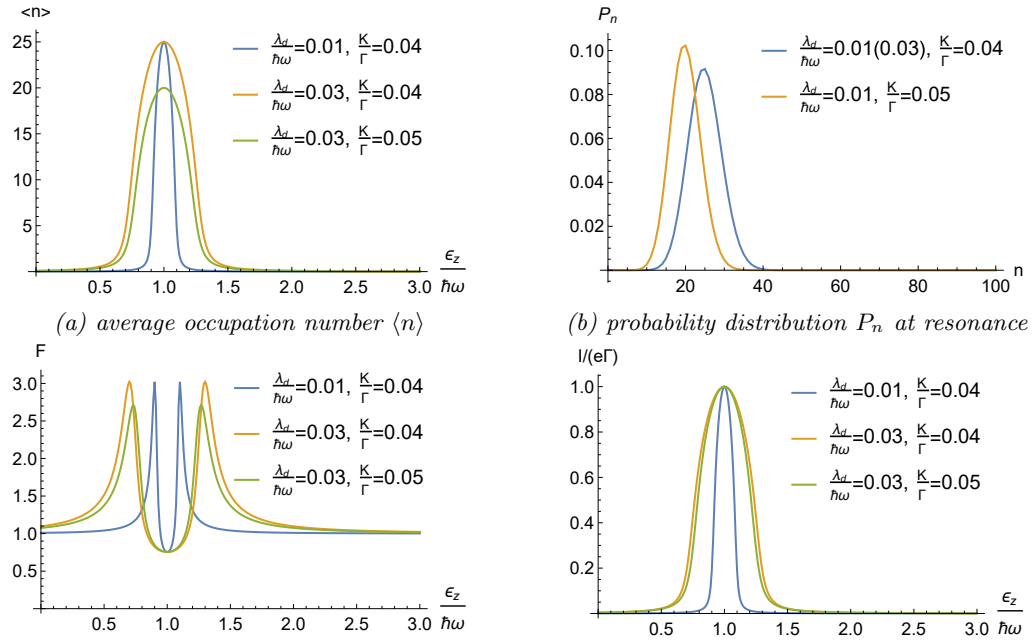

(a) average occupation number $\langle n\rangle$

(b) probability distribution P_n at resonance

(c) Fano factor $F = \frac{\langle(\Delta n)^2\rangle}{\langle n\rangle}$

(d) the current I in $e\Gamma$ units

Figure 5: Numerical simulation results demonstrate the single-atom lasing effect when the left lead has full spin up polarisation and the right lead has the opposite, i.e. $p = p_L = -p_R = 1$, $\hat{n}_L = \hat{n}_R = \hat{e}_z$. (a) The system reaches a non-equilibrium steady state with the oscillation occupation number larger than zero at resonance. (b) and (c) The probability distribution at resonance observes a sharp peak with the Fano factor smaller than zero, indicating the characteristic sub-Poissonian statistics for single-atom lasers. (d) The quantum dot acts as a spin valve allowing maximum current at resonance.

The numerical simulation results in Figure (5) demonstrate the phonon lasing effect.

The non-zero occupation number at resonance in Figure (5a) indicates the heating up of the resonator. The peak broadens as the interaction strength λ_d increases. In addition, the height of the peak decreases for stronger coupling strength K to the bath relative to the lead Γ, reflecting the competition dynamics discussed before.

Figure (5b) shows the probability distributions for the Fock states of the oscillator $|n\rangle$ at resonance. To better understand the distributions, we calculated the Fano factor of each distribution with different parameters in Figure (5c). The Fano factor is defined as $F = \frac{\langle(\Delta n)^2\rangle}{\langle n\rangle}$. For a Poisson process, the Fano factor equals to one. In Figure (5c), at resonance, the Fano factor is the same for all distributions with different parameters and is smaller than one, indicating Sub-Poissonian

statistics, which is an evidence of single-atom lasing effect compared to the case of heating.

The current in Figure (5d) shows the electron transport property of the system. As discussed before, without the interaction between the dot and the oscillator (e.g. when the value of $\frac{\epsilon_z}{\hbar\omega}$ is far from one), there cannot be any current in the system. The current reaches its peak value when $\frac{\epsilon_z}{\hbar\omega} = 1$, indicating a strong spin-flip interaction between the dot and the oscillator at resonance.

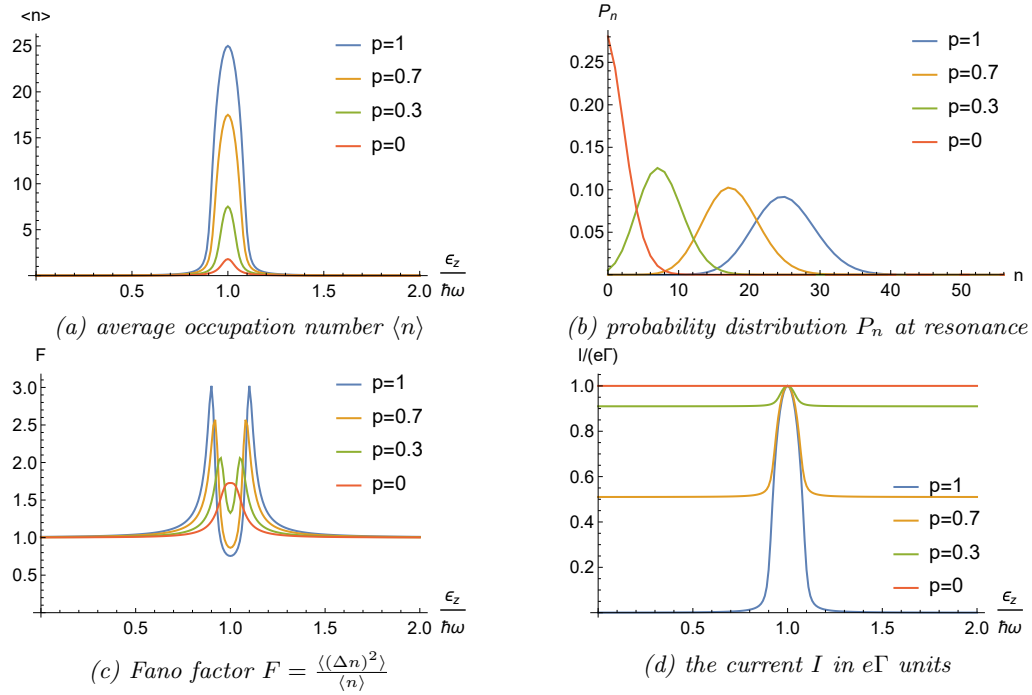

(a) average occupation number $\langle n \rangle$

(b) probability distribution P_n at resonance

(c) Fano factor $F = \frac{\langle (\Delta n)^2 \rangle}{\langle n \rangle}$

(d) the current I in $e\Gamma$ units

Figure 6: Numerical simulation results when the leads are polarised in antiparallel configuration as before but with different polarisation strengths. Here $\frac{\lambda_d}{\hbar\omega} = 0.01$, $\frac{K}{\Gamma} = 0.04$. The system demonstrates the single-atom lasing effect as long as the leads are sufficiently polarised.

Figure (6) demonstrates that even if the leads are not fully polarised in antiparallel configuration, the oscillator can still reach a non-equilibrium steady state with the phonon occupation number larger than zero (Figure (6a)), and as long as the polarisation is strong enough, the system can be characterised by sub-Poissonian statistics at resonance (Figure (6b) and (6c)). The quantum dot keeps acting as a spin-valve until $p = 0$ as the polarisation strength decreases (Figure (6d)).

3 Non-collinearly Polarised Leads

3.1 The Hamiltonian and the Eigenstates

When the leads are non collinearly polarised, we re-define the quantisation axis of the dot spin as $\hat{e}_x = \hat{n}_L + \hat{n}_R$, $\hat{e}_y = \hat{n}_L - \hat{n}_R$ and $\hat{e}_z = \hat{n}_L \times \hat{n}_R$. We assume the quantum dot can only exchange energy with the oscillator by flipping its spin in the $\hat{e}_x$ direction, because, e.g. the external magnetic field is exerted on the dot in $\hat{e}_x$ direction. Still taking $|\alpha, n\rangle$ as the basis, where α is the spin state

in $\hat{e}_z$ direction as usual, the interaction Hamiltonian between the dot and the oscillator can be re-written as:

$$\begin{aligned}\hat{H}_{\text{int,dot}} =& -\lambda_d \left(\hat{d}^\dagger_{\downarrow_x}\hat{d}_{\uparrow_x} + \hat{d}^\dagger_{\uparrow_x}\hat{d}_{\downarrow_x}\right)\left(\hat{b}^\dagger + \hat{b}\right)\\ =& -\frac{\lambda_d}{2}\left[\left(\hat{d}^\dagger_\uparrow + \hat{d}^\dagger_\downarrow\right)\left(\hat{d}_\uparrow - \hat{d}_\downarrow\right) + \left(\hat{d}^\dagger_\uparrow - \hat{d}^\dagger_\downarrow\right)\left(\hat{d}_\uparrow + \hat{d}_\downarrow\right)\right]\left(\hat{b}^\dagger + \hat{b}\right).\end{aligned}$$

The tunnelling Hamiltonian between the leads and the quantum dot becomes [23]:

$$\hat{H}_{\text{tun},leads} = \sum_{\eta k}\frac{V_\eta}{\sqrt{2}}\left[\hat{c}^\dagger_{\eta k+}\left(e^{i\frac{\phi_\eta}{2}}\hat{d}_\uparrow + e^{-i\frac{\phi_\eta}{2}}\hat{d}_\downarrow\right) + \hat{c}^\dagger_{\eta k-}\left(-e^{i\frac{\phi_\eta}{2}}\hat{d}_\uparrow + e^{-i\frac{\phi_\eta}{2}}\hat{d}_\downarrow\right)\right] + H.c.\ ,$$

where $\hat{c}^\dagger_{\eta k\pm}$ ($\hat{c}_{\eta k\pm}$) is the creation (annihilation) operator of an electron with its spin in the polarisation direction (+) of the lead η or the opposite (-), and $\phi_L = -\phi_R = \frac{\phi}{2}$, where $\phi = \sphericalangle(\hat{n}_L, \hat{n}_R)$ is the angle between the two leads' magnetisations. We redefine $p_\eta = \frac{\rho_{\eta+}-\rho_{\eta-}}{\rho_{\eta+}+\rho_{\eta-}} \in [-1,1]$, $\Gamma_{\eta\pm} = \Gamma_\eta(1\pm p_\eta)$, and $\Gamma_\eta = \frac{\Gamma_{\eta+}+\Gamma_{\eta-}}{2}$.

Under the RWA, the eigenstates are $|0,n\rangle$, $|D,n\rangle$ and:

$$\begin{aligned}|+,n\rangle =& \sin\theta_n\,|\uparrow_x,n\rangle - \cos\theta_n\,|\downarrow_x,n+1\rangle\\ =& \frac{\sin\theta_n}{\sqrt{2}}(|\uparrow,n\rangle + |\downarrow,n\rangle) - \frac{\cos\theta_n}{\sqrt{2}}(|\uparrow,n+1\rangle - |\downarrow,n+1\rangle),\\ |-,n\rangle =& \cos\theta_n\,|\uparrow_x,n\rangle + \sin\theta_n\,|\downarrow_x,n+1\rangle\\ =& \frac{\cos\theta_n}{\sqrt{2}}(|\uparrow,n\rangle + |\downarrow,n\rangle) + \frac{\sin\theta_n}{\sqrt{2}}(|\uparrow,n+1\rangle - |\downarrow,n+1\rangle),\end{aligned}$$

3.2 Reduced Density Matrix and the Master Equation

Same as in the collinear case, we integrate out the non-interacting degrees of freedom of the leads and the bath to obtain the reduced density matrix $\hat{\rho}$ for the coupled system with the dot and the oscillator:

$$\hat{\rho} = \sum_{\chi_1,n_1;\chi_2,n_2} P^{\chi_1,n_1}_{\chi_2,n_2}\,|\chi_2,n_2\rangle\langle\chi_1,n_1|\,.$$

The matrix element is defined as $P^{\chi_1,n_1}_{\chi_2,n_2} = \langle\chi_2,n_2|\,\hat{\rho}\,|\chi_1,n_1\rangle$, hence $P^{\chi_2,n_2}_{\chi_1,n_1} = \left(P^{\chi_1,n_1}_{\chi_2,n_2}\right)^*$. The diagonal, real terms $P_{\chi,n} = P^{\chi,n}_{\chi,n}$ are simply the probabilities of the system being in the corresponding state $|\chi,n\rangle$.

The spin of the electron is no longer conserved in individual tunnelling events between the dot and the ferromagnetic leads, because an electron tunnelling from the leads to the dot is in fact in

superposition of $|\uparrow_x\rangle$ and $|\downarrow_x\rangle$. Therefore, we get off-diagonal terms in the reduced density matrix:

$$\begin{pmatrix}
P_{0,n-1} & 0 & 0 & 0 & 0 & 0 & 0 & 0 & 0 & 0 & 0 & 0 \\
0 & P_{+,n-1} & 0 & 0 & 0 & P^{+,n-1}_{+,n} & P^{+,n-1}_{-,n} & 0 & 0 & 0 & 0 & 0 \\
0 & 0 & P_{-,n-1} & 0 & 0 & P^{-,n-1}_{+,n} & P^{-,n-1}_{-,n} & 0 & 0 & 0 & 0 & 0 \\
0 & 0 & 0 & P_{D,n-1} & 0 & 0 & 0 & 0 & 0 & 0 & 0 & 0 \\
0 & 0 & 0 & 0 & P_{0,n} & 0 & 0 & 0 & 0 & 0 & 0 & 0 \\
0 & P^{+,n}_{+,n-1} & P^{+,n}_{-,n-1} & 0 & 0 & P_{+,n} & 0 & 0 & 0 & P^{+,n}_{+,n+1} & P^{+,n}_{-,n+1} & 0 \\
0 & P^{-,n}_{+,n-1} & P^{-,n}_{-,n-1} & 0 & 0 & 0 & P_{-,n} & 0 & 0 & P^{-,n}_{+,n+1} & P^{-,n}_{-,n+1} & 0 \\
0 & 0 & 0 & 0 & 0 & 0 & 0 & P_{D,n} & 0 & 0 & 0 & 0 \\
0 & 0 & 0 & 0 & 0 & 0 & 0 & 0 & P_{0,n+1} & 0 & 0 & 0 \\
0 & 0 & 0 & 0 & 0 & P^{+,n+1}_{+,n} & P^{+,n+1}_{-,n} & 0 & 0 & P_{+,n+1} & 0 & 0 \\
0 & 0 & 0 & 0 & 0 & P^{-,n+1}_{+,n} & P^{-,n+1}_{-,n} & 0 & 0 & 0 & P_{-,n+1} & 0 \\
0 & 0 & 0 & 0 & 0 & 0 & 0 & 0 & 0 & 0 & 0 & P_{D,n+1}
\end{pmatrix}$$

The time evolution of this reduced density matrix satisfies the following generalised master equation in the stationary limit:

$$0 = \dot{P}^{\chi_1,n_1}_{\chi_2,n_2} = -\frac{i}{\hbar}(E_{\chi_1,n_1} - E_{\chi_2,n_2})P^{\chi_1,n_1}_{\chi_2,n_2} + \sum_{\chi_1',n_1';\chi_2',n_2'} W^{\chi_1,n_1;\chi_1',n_1'}_{\chi_2,n_2;\chi_2',n_2'} P^{\chi_1',n_1'}_{\chi_2',n_2'}, \tag{4}$$

where $W^{\chi_1,n_1;\chi_1',n_1'}_{\chi_2,n_2;\chi_2',n_2'}$ is the generalised transition rate in Liouville space. The first term on the right hand side accounts for the coherent evolution of the reduced system, and the second term describes the dissipative coupling to the leads and the thermal bath.

3.3 Transition Rates, Current and Diagrammatic Rules

As there are off-diagonal terms in the reduced density matrix, and Fermi Golden Rules are only applicable for the transition rates involving diagonal terms, we need to apply the diagrammatic perturbation theory [24, 25] to obtain all the general transition rates.

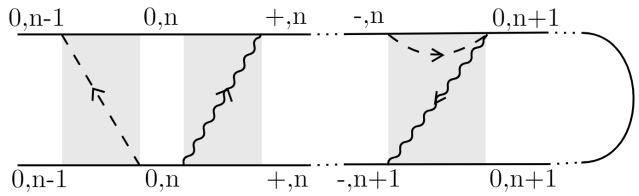

Figure 7: The diagram with Keldysh formalism. The firm straight line is the Keldysh contour, where the eigenstates $|\chi, n\rangle$ propagates. The dashed lines are the leads electron tunnelling lines; the zigzag lines are the bath phonon tunnelling lines. The shaded rectangles are the self-energy blocks.

When the coupling to the leads and the thermal bath is weak, the general transition rates $W^{\chi_1,n_1;\chi_1',n_1'}_{\chi_2,n_2;\chi_2',n_2'}$ can be evaluated in perturbation expansions in the coupling strength Γ and K. They are defined as the irreducible self-energy blocks of the dot-oscillator propagator on a Keldysh contour as shown in Figure (8).

The current through the lead η can be calculated by:

$$\hat{I}_\eta = -e\frac{d\hat{N}_\eta}{dt} = ie\left[\hat{H}, \hat{N}_\eta\right] = -ie\hat{H}_{\text{tun},\eta},$$

where $\hat{N}_\eta$ is the electron number operator of lead η. Therefore, we can define

$$I_\eta = \sum_{\chi,n;\chi_1',n_1';\chi_2',n_2'} W^{\chi,n;\chi_1',n_1' I_\eta}_{\chi,n;\chi_2',n_2'} P^{\chi_1',n_1'}_{\chi_2',n_2'},$$

where $W^{\chi,n;\chi_1',n_1' I_\eta}_{\chi,n;\chi_2',n_2'}$ can be calculated diagrammatically as general current rates in a similar way to $W^{\chi_1,n_1;\chi_1',n_1'}_{\chi_2,n_2;\chi_2',n_2'}$ with a factor difference.

The diagrammatic rule for the general transition rates and general current rates is as follows:

1. Draw all topologically different diagrams with vertices and propagators. Assign states $|\chi, n\rangle$ and corresponding energies $E_{\chi,n}$ to the vertices and all propagators. Assign energy ω_i to all tunnelling lines. The vertices are contracted pairwisely by lead electron tunnelling lines and/or bath phonon tunnelling lines. The lead tunnelling lines either conserve or flip the spin; the bath tunnelling lines conserve the phonon number (one).

2. For each part of the diagram between adjacent vertices assign a resolvent $\frac{1}{\Delta E + i0+}$, where ΔE is the energy difference between left-going and right-going propagators and tunnelling lines.

3. (a) For each lead tunnelling line involving the ferromagnetic lead η, the diagram acquires a factor of $\frac{\Gamma_\eta}{2\pi} f_\eta^{\pm}(\omega_i)$ if it does not flip the spin of the tunnelling electron. If it flips the spin from up to down, the diagram acquires a factor of $\frac{p_\eta \Gamma_\eta}{2\pi} e^{i\phi_\eta} f_\eta^{\pm}(\omega_i)$. Flipping the spin in the opposite direction give rise to the complex conjugate of the aforementioned factor. Here, the $-(+)$ sign refers to lines running forward (backward) with respect to the Keldysh contour.

   (b) For each bath tunnelling line, the diagram acquires a factor of $\frac{K}{2\pi}$.

4. (a) For each vertex that annihilates (creates) a dot electrons with spin σ, the diagram is multiplied by $\langle\chi_2, n_2|\,\hat{c}_\sigma\,|\chi_1, n_1\rangle$ ($\langle\chi_2, n_2|\,\hat{c}_\sigma^\dagger\,|\chi_1, n_1\rangle$), where $|\chi_1, n_1\rangle$ and $|\chi_2, n_2\rangle$ are the states that enter and leaves the vertex, respectively.

   (b) For each vertex that annihilates (creates) a phonon, the diagram is multiplied by $\langle\chi_2, n_2|\,\hat{b}\,|\chi_1, n_1\rangle$ ($\langle\chi_2, n_2|\,\hat{b}^\dagger\,|\chi_1, n_1\rangle$), where $|\chi_1, n_1\rangle$ and $|\chi_2, n_2\rangle$ are the states that enter and leaves the vertex, respectively.

5. The diagram is multiplied by a factor of $(-i)(-1)^{a+b}$, where a is the number of vertices on the lower propagator and b is the number of crossings of tunnelling lines.

6. When calculating the generalised current rates, multiply each diagram by (i) 1 if the electron tunnelling line is going form the lower to the upper propagator (ii) -1 if the electron tunnelling line is going from the upper to the lower propagator (iii) 0 otherwise.

7. Integrate over the energies of the tunnelling lines ω_i and sum over all diagrams.

3.4 First Order Expansion

In this work, we analyse the system in first order expansion. Therefore, we only consider self-energy blocks with one tunnelling line.

We assume that $\Gamma, \mathrm{K} \ll \lambda_d \ll \hbar\omega$. In first order expansion, for all the non-zero off-diagonal terms, $E_{\chi_1,n_1} - E_{\chi_2,n_2}$ is of the order of $\hbar\omega$, while $W^{\chi_1,n_1;\chi_1',n_1'}_{\chi_2,n_2;\chi_2',n_2'}$ is of the order of Γ or K. Hence Equation (4) reduces to

$$0 = \dot{P}^{\chi_1,n_1}_{\chi_2,n_2} = -\frac{i}{\hbar}(E_{\chi_1,n_1} - E_{\chi_2,n_2})P^{\chi_1,n_1}_{\chi_2,n_2}.$$

Therefore, all the off-diagonal terms $P^{\chi_1,n_1}_{\chi_2,n_2}$ are reduced to zero, hence we expect the results obtained from the diagrammatic rule in first order expansion to agree with those from Fermi Golden Rules.

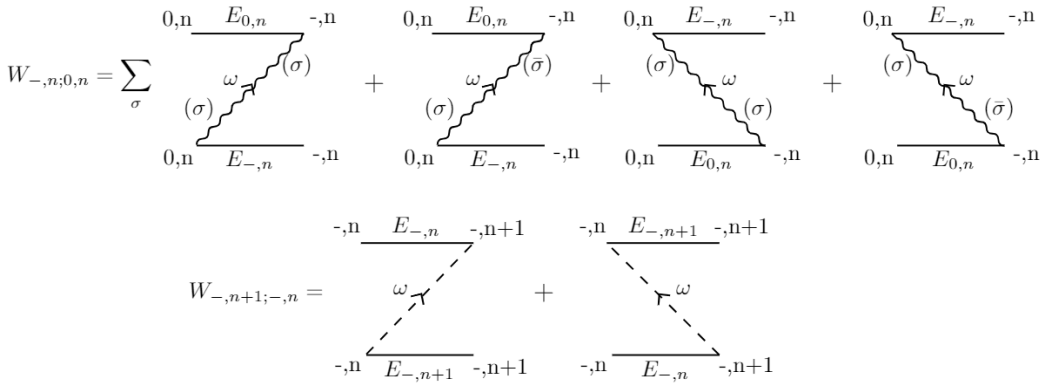

Figure 8: Two examples of general transition rates in first order expansion. The upper one involves the leads electron tunnelling line, and the bottom one involves the bath phonon tunnelling line.

3.5 Results

We calculated the first order general transition rates for the non-collinear case and they are listed in Appendix B.1. The corresponding general transition rates under uni-directional transport assumption are listed in Appendix B.2.

By comparing the above general transition rates to the transition rates calculated for the collinear polarised case in Appendix A.2, we can derive a transformation rule for the transition rates from collinear to non-collinear case: $\Gamma_{\eta,\uparrow/\downarrow} = \Gamma_{\mathrm{L}}(1 \pm p_\eta \cos\phi)$. This makes good geometric sense as now the coupling strength to the leads depends on the angle between the magnetisations and the spin-flip axis.

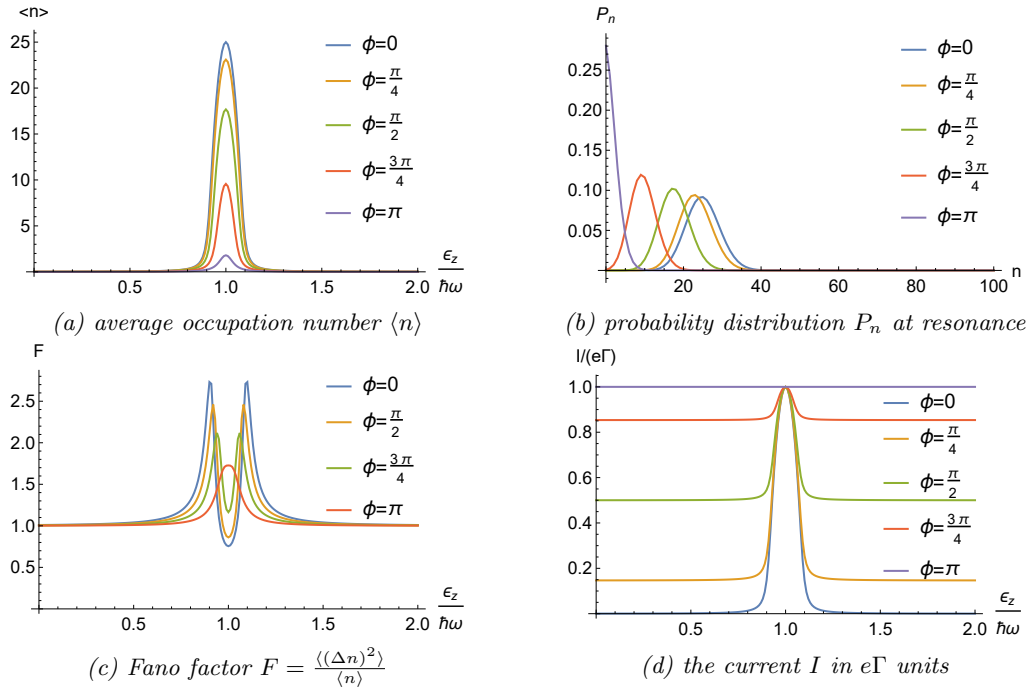

(a) average occupation number $\langle n \rangle$

(b) probability distribution P_n at resonance

(c) Fano factor $F = \frac{\langle (\Delta n)^2 \rangle}{\langle n \rangle}$

(d) the current I in $e\Gamma$ units

Figure 9: First order numerical simulation results where the leads are non-collinearly polarised, and $p_L = -p_R = 1$, $\frac{\lambda_d}{\hbar\omega} = 0.01$, $\frac{K}{\Gamma} = 0.04$. The graphs here resemble key characteristics of the graphs with different polarisation strength in Figure (6).

As shown in Figure (9), in the first order expansion approximation, we can observe the phonon lasing effect in this dot-oscillator system as long as the angle between the magnitisations are sufficiently small and the leads are fully polarised.

Besides, the numerical simulation results for different angles between the two leads as shown in Figure (9) are very similar to the the results for the antiparallelly polarised case with different polarisation strength as shown in Figure (6). This is not surprising because the spin state in the non-collinearly polarised lead can be viewed as a superposition state of $|\uparrow_x\rangle$ and $|\downarrow_x\rangle$, which is similar to the case when the lead are antiparallelly polarised with both $|\uparrow_x\rangle$ and $|\downarrow_x\rangle$ states.

Also, from the transformation rule mentioned before, it is not hard to deduce that when the angle between the magnetisation of the two leads is ϕ, the first order results are the same as the antiparallel polarisation case with $p = \cos\frac{\phi}{2}$.

4 Discussion and Conclusions

In this project, we first reproduced the single-atom lasing effect in the system where a carbon-nanotube quantum dot is suspended between two magnetised leads in antiparallel configuration shown by Mantovani et al. [22]. The system exhibits a sub-Poissonian distribution with sufficiently large polarisation strength. The phonon lasing effect of the system is also manifested in the charge flowing through the dot, which acts as a spin-valve that allows maximum current at resonance between the energy splitting of dot spin states and the intrinsic oscillation mode.

We further explored the situation where the leads are not collinearly polarised. We noticed that there are off-diagonal terms in the reduced density matrix describing the coupled system between the dot and the oscillator, hence a diagrammatic rule was developed to calculate the general transition rates between the elements in the reduced density matrix. We applied the diagrammatic rule to the first order expansion in the electron and phonon tunnelling lines, where all off-diagonal entries vanishes and the results agreed with the ones calculated purely from Fermi Golden Rules. Besides, the numerical simulation of the non-collinear case in the first order resembles features in the antiparallel case with finite polarisation, and shows the single-atom lasing effect when the angle between the polarisation in two leads is sufficiently small.

There are several possible directions for future work on this system.

One is to go beyond the first order expansion and take the off-diagonal terms into consideration. Thus we can utilise the diagrammatic rules developed in this project and understand subtler physics hidden in the case where the leads are non-collinearly polarised.

The other direction is to go beyond the rotation wave approximation. It has been derived that in the case with collinearly polarised leads, the current system can achieve multistable phonon lasing [22]. It would be interesting to explore how this multistability changes when the leads are non-collinearly polarised, as not perfectly collinearly polarised leads are more realistic in practice.

We can also set the bath temperature higher than zero to try both heating up and cooling down effect on the oscillator by manipulating the polarisation of the two leads in the non-collinear polarised case. We expect that the oscillator can be cooled to the ground state when the leads are sufficiently polarised in antiparallel configuration or when the angle between the magnitisations is sufficiently small with full polarisation strength. This is very similar to what we demonstrated here, but it will have different experimental applications from the single-atom lasers.

References

[1] J. McKeever, A. Boca, A. D. Boozer, J. R. Buck, and H. J. Kimble. Experimental realization of a one-atom laser in the regime of strong coupling. *Nature*, 425(6955):268–271, 2003.

[2] P. Filipowicz, J. Javanainen, and P. Meystre. Theory of a microscopic maser. *Phys. Rev. A*, 34:3077–3087, Oct 1986.

[3] Perry R. Rice and H. J. Carmichael. Photon statistics of a cavity-qed laser: A comment on the laser–phase-transition analogy. *Phys. Rev. A*, 50:4318–4329, Nov 1994.

[4] Yi Mu and C. M. Savage. One-atom lasers. *Phys. Rev. A*, 46:5944–5954, Nov 1992.

[5] D. Meschede, H. Walther, and G. Müller. One-atom maser. *Phys. Rev. Lett.*, 54:551–554, Feb 1985.

[6] Kyungwon An, James J. Childs, Ramachandra R. Dasari, and Michael S. Feld. Microlaser: A laser with one atom in an optical resonator. *Phys. Rev. Lett.*, 73:3375–3378, Dec 1994.

[7] X. Mi, J. V. Cady, D. M. Zajac, P. W. Deelman, and J. R. Petta. Strong coupling of a single electron in silicon to a microwave photon. *Science*, 355(6321):156–158, 2017.

[8] Pei-Qing Jin, Michael Marthaler, Jared H Cole, Alexander Shnirman, and Gerd Schn. Lasing and transport in a coupled quantum dot–resonator system. *Physica Scripta*, T151:014032, nov 2012.

[9] L. Childress, A. S. Sørensen, and M. D. Lukin. Mesoscopic cavity quantum electrodynamics with quantum dots. *Phys. Rev. A*, 69:042302, Apr 2004.

[10] Gianluca Rastelli and Michele Governale. Single atom laser in normal-superconductor quantum dots. *arXiv e-prints*, page arXiv:1904.12278, Apr 2019.

[11] Manas Kulkarni, Ovidiu Cotlet, and Hakan E. Türeci. Cavity-coupled double-quantum dot at finite bias: Analogy with lasers and beyond. *Phys. Rev. B*, 90:125402, Sep 2014.

[12] J. J. Viennot, M. C. Dartiailh, A. Cottet, and T. Kontos. Coherent coupling of a single spin to microwave cavity photons. *Science*, 349(6246):408–411, 2015.

[13] Y.-Y. Liu, J. Stehlik, C. Eichler, M. J. Gullans, J. M. Taylor, and J. R. Petta. Semiconductor double quantum dot micromaser. *Science*, 347(6219):285–287, 2015.

[14] Y.-Y. Liu, J. Stehlik, C. Eichler, X. Mi, T. R. Hartke, M. J. Gullans, J. M. Taylor, and J. R. Petta. Threshold dynamics of a semiconductor single atom maser. *Phys. Rev. Lett.*, 119:097702, Aug 2017.

[15] D. A. Rodrigues, J. Imbers, and A. D. Armour. Quantum dynamics of a resonator driven by a superconducting single-electron transistor: A solid-state analogue of the micromaser. *Phys. Rev. Lett.*, 98:067204, Feb 2007.

[16] Shimon Kolkowitz, Ania C. Bleszynski Jayich, Quirin P. Unterreithmeier, Steven D. Bennett, Peter Rabl, J. G. E. Harris, and Mikhail D. Lukin. Coherent sensing of a mechanical resonator with a single-spin qubit. *Science*, 335(6076):1603–1606, 2012.

[17] A. Benyamini, A. Hamo, S. Viola Kusminskiy, F. von Oppen, and S. Ilani. Real-space tailoring of the electron-phonon coupling in ultraclean nanotube mechanical resonators. *Nature Physics*, 10:151 EP –, Jan 2014. Article.

[18] A. V. Parafilo, S. I. Kulinich, L. Y. Gorelik, M. N. Kiselev, R. I. Shekhter, and M. Jonson. Spin-mediated photomechanical coupling of a nanoelectromechanical shuttle. *Phys. Rev. Lett.*, 117:057202, Jul 2016.

[19] P. Stadler, W. Belzig, and G. Rastelli. Ground-state cooling of a carbon nanomechanical resonator by spin-polarized current. *Phys. Rev. Lett.*, 113:047201, Jul 2014.

[20] P. Stadler, W. Belzig, and G. Rastelli. Control of vibrational states by spin-polarized transport in a carbon nanotube resonator. *Phys. Rev. B*, 91:085432, Feb 2015.

[21] G. Rastelli and W. Belzig. Ground state cooling of nanomechanical resonators by electron transport. *The European Physical Journal Special Topics*, 227(15):1885–1895, Mar 2019.

[22] Mattia Mantovani, Andrew D. Armour, Wolfgang Belzig, and Gianluca Rastelli. Dynamical multistability in a quantum-dot laser. *Phys. Rev. B*, 99:045442, Jan 2019.

[23] Jürgen König and Jan Martinek. Interaction-driven spin precession in quantum-dot spin valves. *Phys. Rev. Lett.*, 90:166602, Apr 2003.

[24] Björn Sothmann, David Futterer, Michele Governale, and Jürgen König. Probing the exchange field of a quantum-dot spin valve by a superconducting lead. *Phys. Rev. B*, 82:094514, Sep 2010.

[25] Matthias Braun, Jürgen König, and Jan Martinek. Theory of transport through quantum-dot spin valves in the weak-coupling regime. *Phys. Rev. B*, 70:195345, Nov 2004.

Appendix A Collinear Transition Rates

A.1 General Results

$$W_{+,n;0,n'} = \sum_\eta f_\eta(E_+)\left(\Gamma_{\eta,\uparrow}\sin^2\theta_n\delta_{n',n}\right) + f_\eta(E_+ - \hbar\omega)\left(\Gamma_{\eta,\downarrow}\cos^2\theta_n\delta_{n',n+1}\right)$$

$$W_{-,n;0,n'} = \sum_\eta f_\eta(E_-)\left(\Gamma_{\eta,\uparrow}\cos^2\theta_n\delta_{n',n}\right) + f_\eta(E_- - \hbar\omega)\left(\Gamma_{\eta,\downarrow}\sin^2\theta_n\delta_{n',n+1}\right)$$

$$W_{0,n;+,n'} = \sum_\eta [1-f_\eta(E_+)]\left(\Gamma_{\eta,\uparrow}\sin^2\theta_n\delta_{n',n}\right) + [1-f_\eta(E_+ - \hbar\omega)]\left(\Gamma_{\eta,\downarrow}\cos^2\theta_{n-1}\delta_{n',n-1}\right)$$

$$W_{0,n;-,n'} = \sum_\eta [1-f_\eta(E_-)]\left(\Gamma_{\eta,\uparrow}\cos^2\theta_n\delta_{n',n}\right) + [1-f_\eta(E_- - \hbar\omega)]\left(\Gamma_{\eta,\downarrow}\sin^2\theta_{n-1}\delta_{n',n-1}\right)$$

$$W_{+,n;\mathrm{D},n'} = \sum_\eta [1-f_\eta(E_\mathrm{D} - E_+)]\left(\Gamma_{\eta,\downarrow}\sin^2\theta_n\delta_{n',n}\right) + [1-f_\eta(E_\mathrm{D} + \hbar\omega - E_+)]\left(\Gamma_{\eta,\uparrow}\cos^2\theta_n\delta_{n',n+1}\right)$$

$$W_{-,n;\mathrm{D},n'} = \sum_\eta [1-f_\eta(E_\mathrm{D} - E_-)]\left(\Gamma_{\eta,\downarrow}\cos^2\theta_n\delta_{n',n}\right) + [1-f_\eta(E_\mathrm{D} + \hbar\omega - E_-)]\left(\Gamma_{\eta,\uparrow}\sin^2\theta_n\delta_{n',n+1}\right)$$

$$W_{\mathrm{D},n;+,n'} = \sum_\eta f_\eta(E_\mathrm{D} - E_+)\left(\Gamma_{\eta,\downarrow}\sin^2\theta_n\delta_{n',n}\right) + f_\eta(E_\mathrm{D} + \hbar\omega - E_+)\left(\Gamma_{\eta,\uparrow}\cos^2\theta_{n-1}\delta_{n',n-1}\right)$$

$$W_{\mathrm{D},n;-,n'} = \sum_\eta f_\eta(E_\mathrm{D} - E_-)\left(\Gamma_{\eta,\downarrow}\cos^2\theta_n\delta_{n',n}\right) + f_\eta(E_\mathrm{D} + \hbar\omega - E_-)\left(\Gamma_{\eta,\uparrow}\sin^2\theta_{n-1}\delta_{n',n-1}\right)$$

$$W_{0,0;\downarrow,0} = \sum_\eta [1-f_\eta(E_\downarrow)]\,\Gamma_{\eta,\downarrow}$$

$$W_{\mathrm{D},0;\downarrow,0} = \sum_\eta f_\eta(E_\uparrow)\Gamma_{\eta,\uparrow}$$

$$W_{0,n_{max};\uparrow,n_{max}} = \sum_\eta [1-f_\eta(E_\uparrow)]\,\Gamma_{\eta,\uparrow}$$

$$W_{\mathrm{D},n_{max};\uparrow,n_{max}} = \sum_\eta f_\eta(E_\downarrow)\Gamma_{\eta,\downarrow}$$

$$W_{0,n;0,n+1} = \mathrm{K}(n+1)$$

$$W_{\mathrm{D},n;\mathrm{D},n+1} = \mathrm{K}(n+1)$$

$$\begin{aligned} W_{+,n;+,n+1} =& \mathrm{K}[(n+1)\sin^2\theta_n\sin^2\theta_{n+1} + (n+2)\cos^2\theta_n\cos^2\theta_{n+1} \\ &+ 2\sqrt{(n+1)(n+2)}\sin\theta_n\sin\theta_{n+1}\cos\theta_n\cos\theta_{n+1}] \end{aligned}$$

$$\begin{aligned} W_{-,n;-,n+1} =& \mathrm{K}[(n+1)\cos^2\theta_n\cos^2\theta_{n+1} + (n+2)\sin^2\theta_n\sin^2\theta_{n+1} \\ &+ 2\sqrt{(n+1)(n+2)}\sin\theta_n\sin\theta_{n+1}\cos\theta_n\cos\theta_{n+1}] \end{aligned}$$

$$\begin{aligned} W_{+,n;-,n+1} =& \mathrm{K}[(n+1)\sin^2\theta_n\cos^2\theta_{n+1} + (n+2)\cos^2\theta_n\sin^2\theta_{n+1} \\ &- 2\sqrt{(n+1)(n+2)}\sin\theta_n\sin\theta_{n+1}\cos\theta_n\cos\theta_{n+1}] \end{aligned}$$

$$\begin{aligned} W_{-,n;+,n+1} =& \mathrm{K}[(n+1)\cos^2\theta_n\sin^2\theta_{n+1} + (n+2)\sin^2\theta_n\cos^2\theta_{n+1} \\ &- 2\sqrt{(n+1)(n+2)}\sin\theta_n\sin\theta_{n+1}\cos\theta_n\cos\theta_{n+1}] \end{aligned}$$

$$
\begin{aligned}
W_{\downarrow,0;+,0} =& \mathrm{K}\cos^2\theta_0 \\
W_{\downarrow,0;-,0} =& \mathrm{K}\sin^2\theta_0 \\
W_{+,n_{max}-1;\uparrow,n_{max}} =& \mathrm{K}n_{max}\sin^2\theta_{n_{max}-1} \\
W_{-,n_{max}-1;\uparrow,n_{max}} =& \mathrm{K}n_{max}\cos^2\theta_{n_{max}-1}
\end{aligned}
$$

A.2 Uni-directional Transport

Only the transition rates involving electron tunnellings are affected by the uni-directional transport assumption. Therefore, the rates only involving phonon tunnellings are the same as those in Appendix A.1 and not listed here.

$$
\begin{aligned}
W_{+,n;0,n'} =& \Gamma_{\mathrm{L},\uparrow}\sin^2\theta_n\delta_{n',n} + \Gamma_{\mathrm{L},\downarrow}\cos^2\theta_n\delta_{n',n+1} \\
W_{-,n;0,n'} =& \Gamma_{\mathrm{L},\uparrow}\cos^2\theta_n\delta_{n',n} + \Gamma_{\mathrm{L},\downarrow}\sin^2\theta_n\delta_{n',n+1} \\
W_{0,n;+,n'} =& \Gamma_{\mathrm{R},\uparrow}\sin^2\theta_n\delta_{n',n} + \Gamma_{\mathrm{R},\downarrow}\cos^2\theta_{n-1}\delta_{n',n-1} \\
W_{0,n;-,n'} =& \Gamma_{\mathrm{R},\uparrow}\cos^2\theta_n\delta_{n',n} + \Gamma_{\mathrm{R},\downarrow}\sin^2\theta_{n-1}\delta_{n',n-1} \\
W_{+,n;\mathrm{D},n'} =& \Gamma_{\mathrm{R},\downarrow}\sin^2\theta_n\delta_{n',n} + \Gamma_{\mathrm{R},\uparrow}\cos^2\theta_n\delta_{n',n+1} \\
W_{-,n;\mathrm{D},n'} =& \Gamma_{\mathrm{R},\downarrow}\cos^2\theta_n\delta_{n',n} + \Gamma_{\mathrm{R},\uparrow}\sin^2\theta_n\delta_{n',n+1} \\
W_{\mathrm{D},n;+,n'} =& \Gamma_{\mathrm{L},\downarrow}\sin^2\theta_n\delta_{n',n} + \Gamma_{\mathrm{L},\uparrow}\cos^2\theta_{n-1}\delta_{n',n-1} \\
W_{\mathrm{D},n,-,n'} =& \Gamma_{\mathrm{L},\downarrow}\cos^2\theta_n\delta_{n',n} + \Gamma_{\mathrm{L},\uparrow}\sin^2\theta_{n-1}\delta_{n',n-1} \\
W_{0,0;\downarrow,0} =& \Gamma_{\mathrm{R},\downarrow} \\
W_{\mathrm{D},0;\downarrow,0} =& \Gamma_{\mathrm{L},\uparrow} \\
W_{0,n_{max};\uparrow,n_{max}} =& \Gamma_{\mathrm{R},\uparrow} \\
W_{\mathrm{D},n_{max};\uparrow,n_{max}} =& \Gamma_{\mathrm{L},\downarrow}
\end{aligned}
$$

Appendix B Non-collinear General Transition Rates in First Order

B.1 General Results

$$
\begin{aligned}
W_{+,n;0,n'} =& \sum_{\eta} f_{\eta}^{+}(E_{+})\Gamma_{\eta}(1+p_{\eta}\cos\phi_{\eta})\sin^{2}\theta_{n}\delta_{n',n} \\
&+ f_{\eta}^{+}(E_{+}-\hbar\omega)\Gamma_{\eta}(1-p_{\eta}\cos\phi_{\eta})\cos^{2}\theta_{n}\delta_{n',n+1} \\
W_{-,n;0,n'} =& \sum_{\eta} f_{\eta}^{+}(E_{-})\Gamma_{\eta}(1+p_{\eta}\cos\phi_{\eta})\cos^{2}\theta_{n}\delta_{n',n} \\
&+ f_{\eta}^{+}(E_{-}-\hbar\omega)\Gamma_{\eta}(1-p_{\eta}\cos\phi_{\eta})\sin^{2}\theta_{n}\delta_{n',n+1} \\
W_{0,n;+,n'} =& \sum_{\eta} f_{\eta}^{-}(E_{+})\Gamma_{\eta}(1+p_{\eta}\cos\phi_{\eta})\sin^{2}\theta_{n}\delta_{n',n} \\
&+ f_{\eta}^{-}(E_{+}-\hbar\omega)\Gamma_{\eta}(1-p_{\eta}\cos\phi_{\eta})\cos^{2}\theta_{n-1}\delta_{n',n-1} \\
W_{0,n;-,n'} =& \sum_{\eta} f_{\eta}^{-}(E_{-})\Gamma_{\eta}(1+p_{\eta}\cos\phi_{\eta})\cos^{2}\theta_{n}\delta_{n',n} \\
&+ f_{\eta}^{-}(E_{-}-\hbar\omega)\Gamma_{\eta}(1-p_{\eta}\cos\phi_{\eta})\sin^{2}\theta_{n-1}\delta_{n',n-1} \\
W_{+,n;\mathrm{D},n'} =& \sum_{\eta} f_{\eta}^{-}(E_{\mathrm{D}}-E_{+})\Gamma_{\eta}(1-p_{\eta}\cos\phi_{\eta})\sin^{2}\theta_{n}\delta_{n',n} \\
&+ f_{\eta}^{-}(E_{\mathrm{D}}+\hbar\omega-E_{+})\Gamma_{\eta}(1+p_{\eta}\cos\phi_{\eta})\cos^{2}\theta_{n}\delta_{n',n+1} \\
W_{-,n;\mathrm{D},n'} =& \sum_{\eta} f_{\eta}^{-}(E_{\mathrm{D}}-E_{-})\Gamma_{\eta}(1-p_{\eta}\cos\phi_{\eta})\cos^{2}\theta_{n}\delta_{n',n} \\
&+ f_{\eta}^{-}(E_{\mathrm{D}}+\hbar\omega-E_{-})\Gamma_{\eta}(1+p_{\eta}\cos\phi_{\eta})\sin^{2}\theta_{n}\delta_{n',n+1} \\
W_{\mathrm{D},n;+,n'} =& \sum_{\eta} f_{\eta}^{+}(E_{\mathrm{D}}-E_{+})\Gamma_{\eta}(1-p_{\eta}\cos\phi_{\eta})\sin^{2}\theta_{n}\delta_{n',n} \\
&+ f_{\eta}^{+}(E_{\mathrm{D}}+\hbar\omega-E_{+})\Gamma_{\eta}(1+p_{\eta}\cos\phi_{\eta})\cos^{2}\theta_{n-1}\delta_{n',n-1} \\
W_{\mathrm{D},n;-,n'} =& \sum_{\eta} f_{\eta}^{+}(E_{\mathrm{D}}-E_{-})\Gamma_{\eta}(1-p_{\eta}\cos\phi_{\eta})\cos^{2}\theta_{n}\delta_{n',n} \\
&+ f_{\eta}^{+}(E_{\mathrm{D}}+\hbar\omega-E_{-})\Gamma_{\eta}(1+p_{\eta}\cos\phi_{\eta})\sin^{2}\theta_{n-1}\delta_{n',n-1} \\
W_{0,0;\downarrow_{x},0} =& \sum_{\eta} f_{\eta}^{-}(E_{\downarrow})\Gamma_{\eta}(1-p_{\eta}\cos\phi_{\eta}) \\
W_{\mathrm{D},0;\downarrow_{x},0} =& \sum_{\eta} f_{\eta}^{+}(E_{\uparrow})\Gamma_{\eta}(1+p_{\eta}\cos\phi_{\eta}) \\
W_{0,n_{max};\uparrow_{x},n_{max}} =& \sum_{\eta} f_{\eta}^{-}(E_{\uparrow})\Gamma_{\eta}(1+p_{\eta}\cos\phi_{\eta}) \\
W_{\mathrm{D},n_{max};\uparrow_{x},n_{max}} =& \sum_{\eta} f_{\eta}^{+}(E_{\downarrow})\Gamma_{\eta}(1-p_{\eta}\cos\phi_{\eta})
\end{aligned}
$$

$$
\begin{aligned}
W_{0,n;0,n+1} =& \mathrm{K}(n+1) \\
W_{\mathrm{D},n;\mathrm{D},n+1} =& \mathrm{K}(n+1) \\
W_{+,n;+,n+1} =& \mathrm{K}[(n+1)\sin^2\theta_n \sin^2\theta_{n+1} + (n+2)\cos^2\theta_n \cos^2\theta_{n+1} \\
& + 2\sqrt{(n+1)(n+2)}\sin\theta_n \sin\theta_{n+1}\cos\theta_n \cos\theta_{n+1}] \\
W_{-,n;-,n+1} =& \mathrm{K}[(n+1)\cos^2\theta_n \cos^2\theta_{n+1} + (n+2)\sin^2\theta_n \sin^2\theta_{n+1} \\
& + 2\sqrt{(n+1)(n+2)}\sin\theta_n \sin\theta_{n+1}\cos\theta_n \cos\theta_{n+1}] \\
W_{+,n;-,n+1} =& \mathrm{K}[(n+1)\sin^2\theta_n \cos^2\theta_{n+1} + (n+2)\cos^2\theta_n \sin^2\theta_{n+1} \\
& - 2\sqrt{(n+1)(n+2)}\sin\theta_n \sin\theta_{n+1}\cos\theta_n \cos\theta_{n+1}] \\
W_{-,n;+,n+1} =& \mathrm{K}[(n+1)\cos^2\theta_n \sin^2\theta_{n+1} + (n+2)\sin^2\theta_n \cos^2\theta_{n+1} \\
& - 2\sqrt{(n+1)(n+2)}\sin\theta_n \sin\theta_{n+1}\cos\theta_n \cos\theta_{n+1}] \\
W_{\downarrow_x,0;+,0} =& \mathrm{K}\cos^2\theta_0 \\
W_{\downarrow_x,0;-,0} =& \mathrm{K}\sin^2\theta_0 \\
W_{+,n_{max}-1;\uparrow_x,n_{max}} =& \mathrm{K}n_{max}\sin^2\theta_{n_{max}-1} \\
W_{-,n_{max}-1;\uparrow_x,n_{max}} =& \mathrm{K}n_{max}\cos^2\theta_{n_{max}-1} \\
W_{\chi,n;\chi,n} =& -\sum_{\chi',n'=\chi.n} W_{\chi',n';\chi.n}
\end{aligned}
$$

B.2 Uni-directional Transport

Similar to the collinear case, the rates only involving phonon tunnellings are the same as those in Appendix B.1 and are not listed here.

$$
\begin{aligned}
W_{+,n;0,n'} =&\Gamma_{\mathrm{L}}(1+p_{\mathrm{L}}\cos\frac{\phi}{2})\sin^2\theta_n\delta_{n',n}+\Gamma_{\mathrm{L}}(1-p_{\mathrm{L}}\cos\frac{\phi}{2})\cos^2\theta_n\delta_{n',n+1}\\
W_{-,n;0,n'} =&\Gamma_{\mathrm{L}}(1+p_{\mathrm{L}}\cos\frac{\phi}{2})\cos^2\theta_n\delta_{n',n}+\Gamma_{\mathrm{L}}(1-p_{\mathrm{L}}\cos\frac{\phi}{2})\sin^2\theta_n\delta_{n',n+1}\\
W_{0,n;+,n'} =&\Gamma_{\mathrm{R}}(1+p_{\mathrm{R}}\cos\frac{\phi}{2})\sin^2\theta_n\delta_{n',n}+\Gamma_{\mathrm{R}}(1-p_{\mathrm{R}}\cos\frac{\phi}{2})\cos^2\theta_{n-1}\delta_{n',n-1}\\
W_{0,n;-,n'} =&\Gamma_{\mathrm{R}}(1+p_{\mathrm{R}}\cos\frac{\phi}{2})\cos^2\theta_n\delta_{n',n}+\Gamma_{\mathrm{R}}(1-p_{\mathrm{R}}\cos\frac{\phi}{2})\sin^2\theta_{n-1}\delta_{n',n-1}\\
W_{+,n;\mathrm{D},n'} =&\Gamma_{\mathrm{R}}(1-p_{\mathrm{R}}\cos\frac{\phi}{2})\sin^2\theta_n\delta_{n',n}+\Gamma_{\mathrm{R}}(1+p_{\mathrm{R}}\cos\frac{\phi}{2})\cos^2\theta_n\delta_{n',n+1}\\
W_{-,n;\mathrm{D},n'} =&\Gamma_{\mathrm{R}}(1-p_{\mathrm{R}}\cos\frac{\phi}{2})\cos^2\theta_n\delta_{n',n}+\Gamma_{\mathrm{R}}(1+p_{\mathrm{R}}\cos\frac{\phi}{2})\sin^2\theta_n\delta_{n',n+1}\\
W_{\mathrm{D},n;+,n'} =&\Gamma_{\mathrm{L}}(1-p_{\mathrm{L}}\cos\frac{\phi}{2})\sin^2\theta_n\delta_{n',n}+\Gamma_{\mathrm{L}}(1+p_{\mathrm{L}}\cos\frac{\phi}{2})\cos^2\theta_{n-1}\delta_{n',n-1}\\
W_{\mathrm{D},n,-,n'} =&\Gamma_{\mathrm{L}}(1-p_{\mathrm{L}}\cos\frac{\phi}{2})\cos^2\theta_n\delta_{n',n}+\Gamma_{\mathrm{L}}(1+p_{\mathrm{L}}\cos\frac{\phi}{2})\sin^2\theta_{n-1}\delta_{n',n-1}\\
W_{0,0;\downarrow_x,0} =&\Gamma_{\mathrm{R}}(1-p_{\mathrm{R}}\cos\frac{\phi}{2})\\
W_{\mathrm{D},0;\downarrow_x,0} =&\Gamma_{\mathrm{L}}(1+p_{\mathrm{L}}\cos\frac{\phi}{2})\\
W_{0,n_{max};\uparrow_x,n_{max}} =&\Gamma_{\mathrm{R}}(1+p_{\mathrm{R}}\cos\frac{\phi}{2})\\
W_{\mathrm{D},n_{max};\uparrow_x,n_{max}} =&\Gamma_{\mathrm{L}}(1-p_{\mathrm{L}}\cos\frac{\phi}{2})\\
W_{\downarrow_x,0;\downarrow_x,0} =&-\Gamma_R\left(1-p_R\cos\frac{\phi}{2}\right)-\Gamma_L\left(1+p_L\cos\frac{\phi}{2}\right)\\
W_{\uparrow_x,n_{\max};\uparrow_x,n_{\max}} =&-\Gamma_R\left(1+p_R\cos\frac{\phi}{2}\right)-\Gamma_L\left(1-p_L\cos\frac{\phi}{2}\right)-\mathrm{K}n_{\max}\\
W_{0,n;0,n} =&-2\Gamma_L-\mathrm{K}n\\
W_{D,n;D,n} =&-2\Gamma_R-\mathrm{K}n\\
W_{+,n;+,n} =&-\left[\Gamma_R\left(1+p_R\cos\frac{\phi}{2}\right)+\Gamma_L\left(1-p_L\cos\frac{\phi}{2}\right)\right]\sin\theta_n{}^2\\
&-\left[\Gamma_R\left(1-p_R\cos\frac{\phi}{2}\right)+\Gamma_L\left(1+p_L\cos\frac{\phi}{2}\right)\right]\cos\theta_n{}^2-\mathrm{K}\left(n+\cos\theta_n{}^2\right)\\
W_{+,n;+,n} =&-\left[\Gamma_R\left(1+p_R\cos\frac{\phi}{2}\right)+\Gamma_L\left(1-p_L\cos\frac{\phi}{2}\right)\right]\cos\theta_n{}^2\\
&-\left[\Gamma_R\left(1-p_R\cos\frac{\phi}{2}\right)+\Gamma_L\left(1+p_L\cos\frac{\phi}{2}\right)\right]\sin\theta_n{}^2-\mathrm{K}\left(n+\sin\theta_n{}^2\right)
\end{aligned}
$$

Appendix C Non-zero Occupation Number when $p = 0$

Note that the occupation number is non-zero even when the leads are not polarised (p=0) as shown in Figure (6a). To better understand this, we calculated the average spin $\langle S_z \rangle$ in the dot and the probability P_s of each eigenstate for $p = 0$ case and compared with $p = 1$ case in Figure (10).

Note that $|\uparrow, n\rangle \approx |-, n\rangle$, $|\downarrow, n\rangle \approx |+, n\rangle$ when $\frac{\epsilon_z}{\hbar\omega} \ll 1$; and $|\uparrow, n\rangle \approx |+, n\rangle$, $|\downarrow, n\rangle \approx |-, n\rangle$ when $\frac{\epsilon_z}{\hbar\omega} \gg 1$.

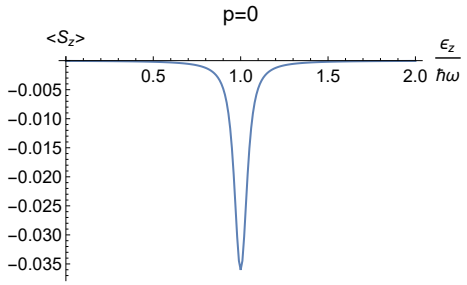

(a) average spin in the dot $\langle S_z \rangle$

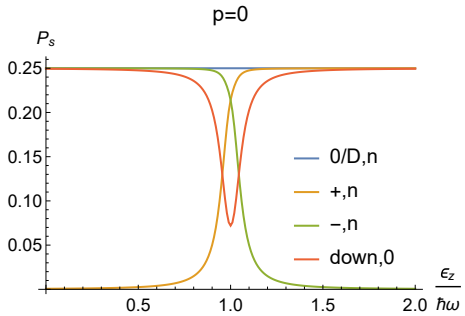

(b) probability of each state P_s

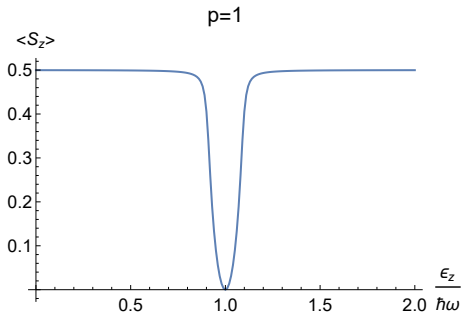

(c) average spin in the dot $\langle S_z \rangle$

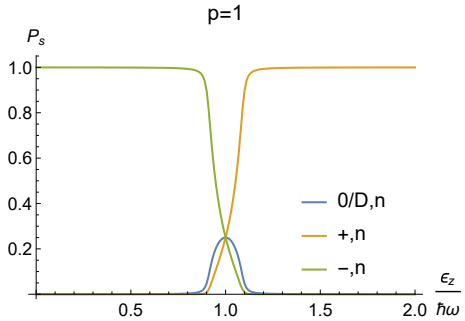

(d) probability of each state P_s

Figure 10: Numerical simulation results for the spin state in the dots when the leads are not polarised ($p = 0$) and fully antiparallelly polarised ($p = 1$). Here $\frac{\lambda_d}{\hbar\omega} = 0.01$, $\frac{K}{\Gamma} = 0.04$. The probability of being in $|\downarrow, 0\rangle$ is always zero when $p = 1$, hence it is not shown in (d).

When $p = 0$ and the value of $\frac{\epsilon_z}{\hbar\omega}$ is far from one, the oscillator can only be at the ground state with $n = 0$, and the probability is equally distributed among $|0, 0\rangle$, $|D, 0\rangle$, $|\uparrow, 0\rangle$ and $|\downarrow, 0\rangle$ as shown in Figure (10b). When the system approaches resonance, due to the interaction λ_d between the dot and the oscillator, the $|\uparrow, 0\rangle$ state can transit to the $|\downarrow, 1\rangle$ state and then to $|0/D, 1\rangle$ and so on, giving rise to the negative average spin in the dot as shown in Figure (10a), the non-zero average phonon occupation number as shown in Figure (6a), and the change in the probability distribution as shown in Figure (10b).

On the contrary, when the leads are fully antiparallelly polarised, the system can only be in $|\uparrow, 0\rangle$ state hence $\langle S_z \rangle = \frac{1}{2}$ when off resonance as shown in Figure (10c) and (10d). When $\frac{\epsilon_z}{\hbar\omega}$ approaches resonance, the interaction between the dot and the oscillator comes into effect, and the system has equal probabilities to be in $|0, n\rangle$, $|D, n\rangle$, $|\uparrow, n\rangle$, and $|\downarrow, n\rangle$ at resonance as shown in Figure (10d), resulting in a zero average spin as shown in Figure (10c).